

An Adjoint-Based Approach for Finding Smooth Surface Waviness Tolerances for Natural Laminar Flow Design

Mohammad Moniripiri^{1,†,*}, Pedro P. C. Brito^{2,*}, André V. G. Cavalieri², Ney R. Sêcco³, Ardeshir Hanifi¹

¹*FLOW, Department of Engineering Mechanics, Royal Institute of Technology, Stockholm, Sweden*

²*Instituto Tecnológico de Aeronáutica, Department of Aerodynamics, São José dos Campos-SP, Brazil*

³*Instituto Tecnológico de Aeronáutica, Department of Aircraft Design, São José dos Campos-SP, Brazil*

First Author Email · momp@kth.se

[†]Corresponding author

*M.M and P.P.C.B contributed equally to this work

Abstract

This work presents a methodology to find manufacturing tolerances for surfaces designed for natural laminar flow to reduce friction drag. The methodology informs the tolerances based on the largest allowable waviness profile with minimum L2-norm of surface deformations that might cause early transition due to the existence of waviness on the surface. The growth of convectively unstable disturbances is computed by solving Euler, compressible boundary layer (BLE), and parabolized stability equations (PSE). The gradient of perturbation energy is found by solving the adjoint of governing equations, and manufacturing tolerances are found using gradient ascent and SLSQP optimization techniques.

1. Introduction

In the 21st century, it is crucial to decrease the specific fuel consumption (SFC) of aircrafts for economic, operational, and ecological reasons. The Advisory Council for Aviation Research and Innovation in Europe (ACARE)¹ has established a number of key goals, one of which is to cut CO₂ emissions per passenger kilometer by 75% by 2050 compared to the levels in 2000. This target has prompted companies to compete in developing new technologies to achieve this reduction.

Some strategies for reducing the SFC are already in place, like the increased propulsion efficiency of engines,² the use of carbon fiber-reinforced materials and composites,³ and the extensive application of multidisciplinary optimizations (MDO)⁴. However, to meet the updated environmental requirements, new strategies for improving aircraft efficiency are demanded. Part of these strategies relies on the design of new vehicle concepts for entry in the next decades,⁵ the implementation of hybrid and electric propulsion systems, and the use of natural laminar flow (NLF) designs. The latter one has the advantage of allowing its application to the current aircraft concepts and significant potential for reducing the SFC. According to Schrauf,⁶ the achievement of laminar flow over 40% of the wings, horizontal and vertical stabilizers, and nacelles surfaces can reduce the total drag by 16%.

Despite advancements in technology enabling manufacturers to create complex surfaces like wings, certain irregularities inevitably arise during the manufacturing and assembly of such structures, and the difficulties regarding the implementation of NLF technology rely on the manufacturing of a sufficiently clean surface, given the discrepancies caused by the significant number of holes, rivets, and fasteners that are usually applied to it. Therefore, analyzing the effect of irregularities, including surface waviness on aerodynamic surfaces, on the boundary layer stability characteristics are important due to their impact on the growth of Tollmien-Schlichting (TS) waves,⁷ that if grow large enough, might cause a sudden transition to turbulence and increase the friction drag and fuel consumption of aircraft. With the concerns mentioned above, the focus of this work is on presenting a practical methodology regarding the information of manufacturing tolerances to guarantee the required surface quality, specifically surface waviness requirement, for designing NLF surfaces.

In the literature, there are different criteria proposed by different researchers for the allowable size of surface irregularities which does not affect the transition, but each has some important limitations. For example, Fage,⁸ using wind tunnel experiments, provided an empirical formula to find allowable sizes of bulges, hollows, and ridges on a flat plate (with a small pressure gradient), and on an airfoil (when the surface irregularity is located in nearly zero pressure gradient region). Fage's experiments were done for a limited range of Reynolds numbers, and also, to use his criterion, the knowledge of transition location in the presence of surface irregularity is necessary which makes the method less

TOLERANCES FOR NATURAL LAMINAR FLOW DESIGN

practical. Carmichael⁹ performed experiments on a two-dimensional wing of an F-94 airplane where full chord laminar flow was maintained by applying suction in the adverse pressure gradient region of the airfoil. Using experimental data, for a waviness located in the favorable pressure gradient region on the airfoil, he proposed an empirical formula that gives the minimum height of waviness (for a specific Reynolds number, wavelength of surface waviness, and chord length) to prevent full-chord NLF in the presence of suction. We also mention the works of Crouch¹⁰ which proposed two correlations concerning the TS type of instabilities for forward and backward facing steps capable of informing the resulted ΔN in the envelope curve, and Perraud¹¹ proposing criteria concerning cross-flow instabilities. Wie and Malik¹² introduced an empirical equation, derived from their numerical calculations, to estimate the change in the N -factor caused by various geometric parameters of waviness, including the number of waves, height, wavelength, as well as the Reynolds number. For more comprehensive information, readers are encouraged to refer to the cited articles.

This study introduces a physics-based numerical framework aimed at determining manufacturing tolerances for smooth waviness on Natural Laminar Flow (NLF) surfaces. The key objective is to identify the critical waviness profile that impacts the transition process. Achieving this involves solving an optimization problem using gradient-based methods. In this work, we adopt the approach proposed by Amoignon *et al.*¹³ to calculate the gradients of kinetic energy of perturbations in the boundary layer with respect to surface deformation, utilizing an adjoint-based method. By solving an unconstrained optimization problem using the gradient ascent method and a constrained problem using the sequential least squares programming (SLSQP) algorithm, we determine the largest permissible surface deformation with the minimum L_2 -norm that induces a specific amplification of disturbances (ΔN), and tolerances are found based on that.

The paper is organized as follows. In the section 2, the procedure to find the sensitivity of objective function for adjoint calculations, together with the governing equations of the problem are explained, and the validation for adjoint implementation is presented in section 3. Section 4 is dedicated to algorithms to find the manufacturing tolerances, and results are presented in section 5. Finally, the main results are concluded in section 6.

2. Methodology and Governing Equations

2.1 Sensitivity Calculation

In this section, an overview of the steps required to calculate the sensitivity of kinetic energy of perturbations inside the boundary layer with respect to surface deformations is given, and in the next section, the governing equations required for each step are explained. To reduce the computational cost, following the method proposed by Amoignon *et al.*,¹³ the viscous boundary layer and the inviscid outer flow are treated separately. However, as will be explained in the following, the boundary layer calculation is dependent on the inviscid region. First, the pressure distribution, C_p , on the airfoil is found by solving Euler equations using ADflow open-source code¹⁴. Approximate Newton-Krylov solver¹⁵ is used to increase the robustness of the solver. After calculating the pressure distribution on the airfoil surface, using an in-house compressible boundary layer code, the meanflow quantities inside the viscous boundary layer are calculated. Finally, for stability analysis, using NOLOT code¹⁶, compressible parabolized stability equations are solved. It should be noted that effects of curvature on stability analysis are taken into account in the PSE calculations. After solving all governing equations, to calculate the desired sensitivities, the adjoint of governing equations, in the reverse order, are solved, i.e. first adjoint of PSE, then adjoint of boundary layer equations, and finally adjoint of Euler equations. To solve the adjoint of boundary layer and PSE, in-house codes¹⁷, and to solve adjoint of Euler equation, ADflow code is used.

2.2 Governing Equations

2.2.1 Inviscid Region: Euler Equations

To solve the inviscid flow around the airfoil, Euler equations are used which in the compact form can be written as

$$\nabla \cdot (\rho \mathbf{U}) = 0, \quad (1)$$

$$\nabla \cdot (\rho \mathbf{U} \mathbf{U}^T) + \nabla p = 0, \quad (2)$$

and

$$\nabla \cdot [\mathbf{U}(E + p)] = 0. \quad (3)$$

In these equations, ρ is density, $\mathbf{U} = [U, V, W]$ is the velocity vector in the inviscid region with U, V and W being its Cartesian components, p is the pressure and E the total energy per unit volume, which is the sum of internal and kinetic energies of the flow. Under the assumption of an ideal and perfect gas, we can write $E = \frac{p}{\gamma-1} + \frac{1}{2}\rho\mathbf{U}^2$ where γ is the specific heat ratio of the gas.

2.2.2 Viscous Region

The total flow inside the BL is decomposed into the mean and disturbance flow quantities as

$$\mathbf{q}_{total}(x^1, x^2, x^3, t) = \bar{\mathbf{q}}(x^1, x^3) + \tilde{\mathbf{q}}(x^1, x^2, x^3, t). \quad (4)$$

$\bar{\mathbf{q}}$ and $\tilde{\mathbf{q}}$ are mean flow and disturbance quantities, and x^1, x^2 , and x^3 are streamwise, spanwise, and wall-normal directions in an orthogonal curvilinear coordinate system, respectively. In such coordinate system, under an infinite swept wing, a length element (ds) is defined by $ds^2 = (dx^1)^2 + (dx^2)^2 + (dx^3)^2$.

2.2.3 Boundary Layer Equations

The quasi-3D non-dimensional compressible BL equations on a swept wing with an infinite span ($\frac{\partial}{\partial x^2} = 0$), in an orthogonal curvilinear coordinate system, are given by equations (5)-(8). All the flow and material quantities (except the pressure,) are made non-dimensional based on chord length, c , and free-stream quantities. Pressure is made non-dimensional with twice the dynamic pressure of the free-stream.

$$\frac{\partial(\bar{\rho}\bar{u})}{\partial x^1} + \frac{\partial(\bar{\rho}\bar{w})}{\partial x^3} = 0 \quad (5)$$

$$\bar{\rho}\bar{u}\frac{\partial\bar{u}}{\partial x^1} + \bar{\rho}\bar{w}\frac{\partial\bar{u}}{\partial x^3} = -\frac{d\bar{p}_e}{dx^1} + \frac{1}{Re}\frac{\partial}{\partial x^3}\left(\bar{\mu}\frac{\partial\bar{u}}{\partial x^3}\right) \quad (6)$$

$$\bar{\rho}\bar{u}\frac{\partial\bar{u}}{\partial x^1} + \bar{\rho}\bar{w}\frac{\partial\bar{v}}{\partial x^3} = \frac{1}{Re}\frac{\partial}{\partial x^3}\left(\bar{\mu}\frac{\partial\bar{v}}{\partial x^3}\right) \quad (7)$$

$$\bar{c}_p\bar{\rho}\bar{T}\frac{\partial\bar{u}}{\partial x^1} + \bar{c}_p\bar{\rho}\bar{w}\frac{\partial\bar{T}}{\partial x^3} = \frac{1}{RePr}\frac{\partial}{\partial x^3}\left(\bar{k}\frac{\partial\bar{T}}{\partial x^3}\right) + \quad (8)$$

$$(\gamma-1)\left\{\bar{u}M^2\frac{d\bar{p}_e}{dx^1} + \frac{\bar{\mu}M^2}{Re}\left[\left(\frac{\partial\bar{u}}{\partial x^3}\right)^2 + \left(\frac{\partial\bar{v}}{\partial x^3}\right)^2\right]\right\}$$

In these equations, $[u, v, w]$ are streamwise, spanwise, and wall-normal velocities, respectively, T is temperature, and ρ is density. Reynolds number, Mach number, and Prandtl number are defined as $Re = \frac{cu_\infty}{\nu_\infty}$, $M = \frac{u_\infty}{\sqrt{\mathcal{R}\gamma T_\infty}}$, and $Pr = \frac{\bar{c}_p\bar{\mu}}{\bar{k}}$, respectively, where c is chord length, u_∞ , ν_∞ , and T_∞ are free-stream velocity, kinematic viscosity, and temperature, respectively. \mathcal{R} is specific gas constant, \bar{c}_p specific heat at constant pressure, γ specific heat ratio, $\bar{\mu}$ dynamic viscosity, and \bar{k} is heat conductivity. Also, p_e is the pressure at BL edge, which under the BL assumptions ($p = p_e(x^1)$), is related to ρ and T through the equation of state as $\gamma M^2 \bar{p}_e = \bar{\rho}\bar{T}$.

2.2.4 Disturbance Equations

The disturbances are decomposed into time- and spanwise periodic waves as

$$\tilde{\mathbf{q}}(x^1, x^2, x^3, t) = \hat{\mathbf{q}}(x^1, x^3)\Theta(x^1, x^2, t), \quad (9)$$

where the wave function, Θ , is defined as

$$\Theta(x^1, x^2, t) = \exp\left\{i\left\{\int_{x_s}^{x^1}\alpha(x')dx' + \beta x^2 - \omega t\right\}\right\}. \quad (10)$$

In equation (10), α is the complex-valued streamwise wavenumber, and β and ω are the real-valued spanwise wavenumber and angular frequency, respectively. Disturbances start to grow from the streamwise location x_s . Assuming BL approximations, there is a scale separation between the weak variation in x^1 and strong variation in x^3 directions, as well as between wall-normal and streamwise mean velocity components. By applying these assumptions and introducing the ansatz (9) into the governing equations, a set of nearly parabolic equations, called Parablized Stability Equations (PSE)¹⁸, will be obtained, which can be written, in symbolic notation, as

$$\mathcal{A}\hat{\mathbf{q}} + \mathcal{B}\frac{\partial\hat{\mathbf{q}}}{\partial x^3} + \mathcal{C}\frac{\partial^2\hat{\mathbf{q}}}{(\partial x^3)^2} + \mathcal{D}\frac{1}{h_1}\frac{\partial\hat{\mathbf{q}}}{\partial x^1} = \mathbf{0}, \quad (11)$$

TOLERANCES FOR NATURAL LAMINAR FLOW DESIGN

where $\hat{q} \in [\hat{\rho}, \hat{u}, \hat{v}, \hat{w}, \hat{T}]^T$, $(h_1)^2 = (\frac{\partial X}{\partial x^1})^2 + (\frac{\partial Y}{\partial x^1})^2 + (\frac{\partial Z}{\partial x^1})^2$, and X, Y , and Z are the Cartesian coordinates. The matrices $\mathcal{A}, \mathcal{B}, \mathcal{C}$ and \mathcal{D} are large 5×5 matrices which can be found in the work of Pralits *et al.*¹⁷. In PSE formulation, both the amplitude $\hat{\mathbf{q}}$ and wave functions depend on x^1 . To remove this ambiguity, and also, to guarantee that variations of $\hat{\mathbf{q}}$ in x^1 -direction remain small allowing to neglect the higher-order streamwise derivatives, a so-called auxiliary condition is used as

$$\int_0^{+\infty} \hat{\mathbf{q}}^H \frac{\partial \hat{\mathbf{q}}}{\partial x^1} dx^3 = 0. \quad (12)$$

Here, superscript H denotes complex conjugate transpose. Equation (11) is integrated downstream with an initial condition at $x^1 = x_s$ given by local stability theory, and at each streamwise location x^1 , the value of α is iterated until the auxiliary condition is satisfied. After finding all the disturbance quantities $\hat{\mathbf{q}}$ and streamwise wavenumber α at all x^1 stations, the perturbation kinetic energy \hat{E} and spatial growth rate σ can be found as

$$\hat{E} = \int_0^{+\infty} \bar{\rho} (|\hat{u}|^2 + |\hat{v}|^2 + |\hat{w}|^2) dx^3, \quad (13)$$

and

$$\sigma = -\alpha_i + \frac{\partial}{\partial x^1} (\ln(\sqrt{\hat{E}})), \quad (14)$$

where α_i is the imaginary part of α . Finally, with the growth rate, the N -factor, which is a measure of integrated growth of perturbations, can be calculated as

$$N = \int_{x_{n1}}^x \sigma dx^1, \quad (15)$$

where x_{n1} is the lower branch of the neutral curve, where disturbance amplification starts ($\sigma = 0$). The N -factor (or growth rate) can then be used in the e^N method¹⁹ to predict the transition location. The combination of Euler, boundary layer, and PSE codes allows a stability analysis of the boundary layers over a given wing section. In what follows we present the procedure to obtain the sensitivity of disturbance energy with respect to surface waviness.

2.3 Flow Case

As mentioned in the introduction, surface waviness might increase the growth of TS waves in the boundary layer and adversely affect the performance of natural laminar flow designs. In this regard, the NLF(2)-0415 natural laminar airfoil²⁰ designed for commuter aircraft applications was chosen for the analysis in this work (figure 1) to investigate how surface waviness may degrade the boundary-layer stability characteristics. Here, the flight conditions are: $M_\infty = 0.5$, $Re = 6 \times 10^6$, and $AoA = 1.25^\circ$. Also, thermodynamic properties of the air were calculated for an altitude of 9600m.

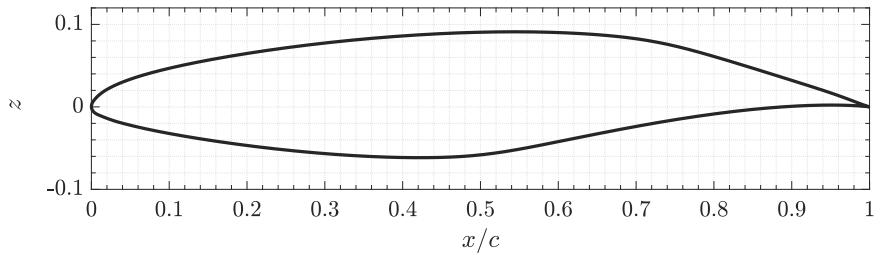


Figure 1: NLF(2)-0415 airfoil.

To solve Euler equations, a C-type structured grid with 1198 grid points (598 volume cells) on the airfoil surface and 69201 total volume cells has been generated using the Construct2D mesh generator code²¹. The computational domain is shown in figure 2a. A farfield boundary condition is set around the domain and a no-penetration boundary condition is used on the airfoil. Since ADflow is a 3D CFD solver, the domain in the spanwise direction has been extruded with 1 volume cell, and at the two sides of the domain, a symmetry boundary condition is used. In figure 2b the generated mesh around the leading edge of the airfoil is shown. It should be noted that, for the purpose of validation of adjoint implementation (as will be discussed in section 3) and to reduce the computational cost of validation process, a mesh with 792 grid points (395 volume cells) on the airfoil has been used; however, the finer grid (with 1198 grid points on the surface) has been used for all other simulations carried out in this work.

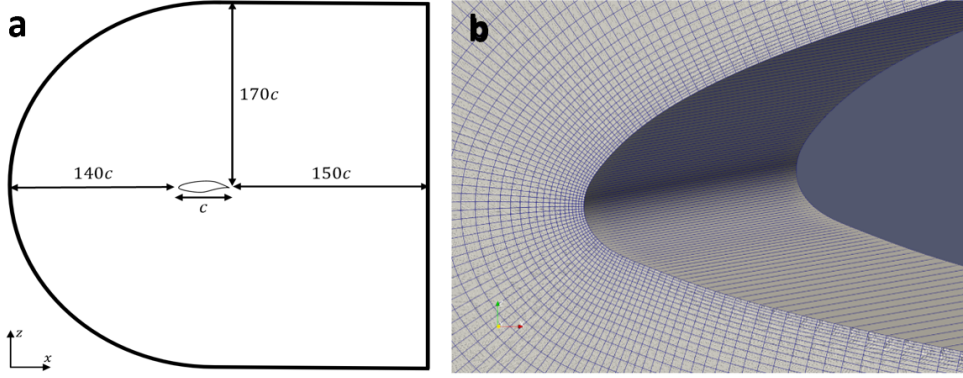


Figure 2: Computational domain (a), generated mesh (b).

2.4 Objective function for sensitivity calculation

To find the surface waviness profile with minimum $L2$ -norm of surface deviations that causes a specific increase in the amplification of perturbations using a gradient-based optimization, the objective function J (to be used in sensitivity calculation) should be a measure of the growth of perturbations in the domain. Here, the kinetic energy of a specific disturbance E_1 , integrated over a selected region, has been chosen for this measure as the objective function. This can be formulated as

$$J(\tilde{\mathbf{q}}, \mathbf{X}) = E_1(\tilde{\mathbf{q}}, \mathbf{X}) = \frac{1}{2} \int_{X_s}^{X_f} \int_{z_0}^{z_1} \int_0^{+\infty} (|\tilde{u}|^2 + |\tilde{v}|^2 + |\tilde{w}|^2) dx^3 dx^2 dx^1. \quad (16)$$

Here, \mathbf{X} is the vector of nodal coordinates, and $[X_s, X_f]$ is the region where the perturbation exists. The amplitudes of disturbances, which are used to calculate the objective function, are the solutions of the PSE (equation (11)) for a specific perturbation mode, which is determined by $\alpha(x_s)$, β , and ω . Here, by computing the envelopes of N -factor curves, we have found the most amplified mode among a wide range of modes with different ω and β , and we have used the disturbance amplitudes of that mode to compute the objective function.

By formulating the objective function J , the sensitivity of the objective function with respect to design variables, which here are taken as all surface grid points and are denoted by \mathbf{z} , can be calculated efficiently using adjoint method. For adjoints of BLE and PSE, we have used a continuous approach. The adjoint equations and their derivations can be found at references such as the works of Pralits *et al.*¹⁷ and Amoignon *et al.*¹³. For adjoint of Euler equations, we have used the discrete adjoint implementation in ADflow code²².

3. Sensitivity Validation

For the purpose of validation, the flight conditions are: $M_\infty = 0.5$, $Re = 6 \times 10^6$, and $AoA = 1.25^\circ$. Also, thermodynamic properties of the air were calculated for an altitude of 9600m. Also for stability calculations, we have chosen an unstable mode with $\beta = 0$, $\alpha_{x_s} = 600 [m^{-1}]$, and frequency (f) equal to 5850Hz. To validate the implementation of the adjoint method, we have compared gradients obtained from the adjoint method with gradients calculated using a central finite difference scheme as given by

$$\frac{\partial J}{\partial g_k} \approx \frac{J(\mathbf{q}(\mathbf{z} + \Delta \mathbf{z}), \mathbf{z} + \Delta \mathbf{z}) - J(\mathbf{q}(\mathbf{z} - \Delta \mathbf{z}), \mathbf{z} - \Delta \mathbf{z})}{2\Delta g_k}. \quad (17)$$

In equation (17), J is the objective function, \mathbf{q} is the state vector (velocity components, pressure, and energy), \mathbf{z} is the surface nodal coordinate vector of the clean airfoil, g_k is the k^{th} design variable, and $\Delta \mathbf{z}$ is the vector of surface deformation (as a result of Δg_k). In equation (17), g_k and the corresponding $\Delta \mathbf{z}$ should be specified. Here, to perturb the geometry, we have parameterized the surface using the so-called Hicks-Henne Bump Functions (HHBFs) and the gradients with respect to a specific control parameter are found. HHBFs are smooth bump functions introduced by Hicks and Henne²³ and are used in aerodynamic shape optimization applications to smoothly modify the shape of the airfoils. They have the analytical definition given by

TOLERANCES FOR NATURAL LAMINAR FLOW DESIGN

$$f_i(\mathbf{x}, a, h, t) = a_i \left[\sin \left(\pi \mathbf{x} \frac{\log(0.5)}{\log(h_i)} \right) \right]^{t_i} = a_i f_{0,i}(\mathbf{x}, h, t), \quad (18)$$

where, \mathbf{x} is the vector of x -coordinates of grid points on the airfoil, and for the i^{th} bump, a_i is the maximum height of the bump, h_i is the x location (based on the chord) where the height of the bump is maximum, and t_i controls the width of the bump. For each set of parameters a , h , and t , the value of HHBF is calculated for all points in \mathbf{x} . The parameterized geometry using HHBFs can be written as

$$z = z_0 + \sum_{i=1}^N a_i f_{0,i}(\mathbf{x}, h, t), \quad (19)$$

where z is the parameterized and z_0 the baseline airfoil geometry, and N the number of HHBFs used to modify the geometry. In equation (17), we have chosen the maximum height of the bump, a , as the design variable, and we deform the airfoil with HHBF, i.e., $g_k = a_k$ and $\Delta \mathbf{z} = \Delta a_k f_{0,k}(\mathbf{x}, h, t) \hat{e}_z$. It should be mentioned that we need to change the position of the bump (using the parameter h), along the surface, and for each position of the bump, the geometry and grid should be updated. To accomplish this, we utilized the IDWarp package²⁴, which uses an inverse distance method to modify the location of mesh volume nodes based on perturbations of the surface nodes. Here, we have calculated the gradients using FD for x/c going from 0.15 to 0.60, which consists of 77 grid points. Also, FD simulations are repeated for 4 different step sizes (Δa) in the range of 10^{-7} to 10^{-4} , and the FD convergence was achieved for $\Delta a = 10^{-5}$. Thus, in total for the central FD method, $77 \times 2 \times 4 = 616$ simulations were performed.

Next, we calculate the sensitivity of the objective function (obtained from adjoint method) with respect to the same design variable as we used in FD, i.e., HHBF height (a). This can be done by putting HHBF centered at all surface grid points and then applying equation (20).

$$\left(\frac{\partial J}{\partial a_i} \right)_{Adjoint} = \int \nabla_z J f_{0,i}(\mathbf{x}, h, t) dx. \quad (20)$$

In this equation, $f_{0,i}(\mathbf{x}, h, t)$ is HHBF with maximum value located at i^{th} grid in x . The comparison of $\nabla_a E = \frac{\partial J}{\partial a}$ obtained from the adjoint method and central finite difference is shown in figure 3. The figure clearly demonstrates the good agreement of the sensitivity obtained using the two methods, confirming the successful implementation of the adjoint method.

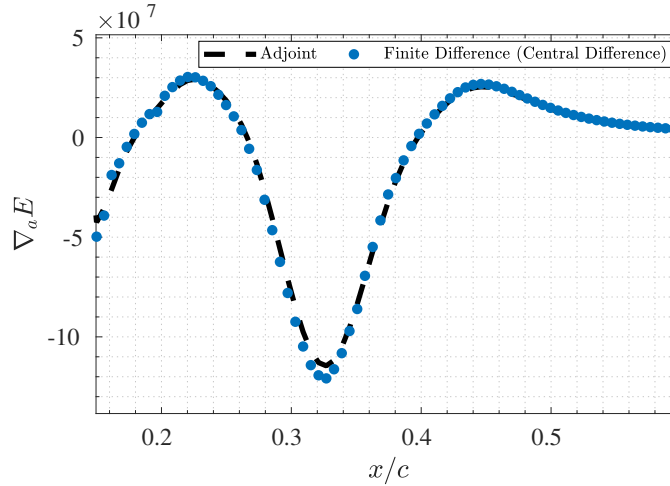


Figure 3: Comparison of gradient obtained using the adjoint method and finite difference ($\Delta a = 10^{-5}$) for upper surface of NLF(2)-0415 airfoil along the chord. $M_\infty = 0.5$, $Re = 6 \times 10^6$, and $AoA = 1.25^\circ$ with $f = 5850\text{Hz}$, $\beta = 0$, $\alpha_{x_s} = 600 [m^{-1}]$.

4. Algorithms for Finding the Manufacturing Tolerances

In order to determine the manufacturing tolerances, it is necessary to identify the maximum allowable waviness profile on airfoil with minimum L_2 -norm of surface deformations that could potentially lead to transition to turbulence due to amplification of TS waves. Minimum L_2 -norm property of this specific waviness profile implies that no other surface

deformation with the same L_2 -norm will induce transition at a particular position along the chord. Once this waviness profile is obtained, the manufacturing tolerances can be calculated. The process of finding this profile involves solving an optimization problem, either unconstrained or constrained, using gradient-based methods, where the adjoint method, which was previously explained, is employed to compute the gradients necessary for this optimization process.

Two optimization problems are solved to determine the desired wavy profiles to find the manufacturing tolerances: an unconstrained optimization problem employing the gradient ascent (GA) method, and a constrained optimization problem utilizing the sequential least squares programming (SLSQP) approach. These choices are motivated by specific factors. The SLSQP approach is capable of identifying the optimal solution, which corresponds to the largest allowable deformation profiles with minimum L_2 -norm of surface deformations. On the other hand, the GA approach offers the advantage of significant saving of computational time at the cost of not finding the optimal solution, but a solution that closely approximates it. The time-saving advantage of GA is because of the fact that GA only requires one computational fluid dynamics (CFD) simulation between each new gradient computation, whereas the SLSQP approach necessitates multiple function evaluations, i.e., CFD simulations, during the search for a new direction which is time-consuming. The subsequent explanations will delve into these two optimization problems and the algorithms employed to solve them.

4.1 Gradient Ascent

The algorithm to find the maximum allowable waviness profile using GA algorithm is explained in the following. Initially, using the stability tools, i.e., the NOLOT code, the growth history of the most unstable mode along the airfoil is obtained. This growth history is represented by the N -factor curve, which serves as a monitoring parameter in our algorithm. Subsequently, we select an allowable increase, denoted as ΔN , in the maximum value of the N -factor. The choice of ΔN is based on the critical value of N utilized in the design of the NLF airfoil. Once ΔN is determined, by taking small steps in the direction of the gradient of E , we will find the waviness profile that increases the maximum value of N -factor by ΔN units, using gradient ascent algorithm which can be written as

$$\mathbf{z}_{n+1} = \mathbf{z}_n + \gamma \frac{\nabla_z E(\mathbf{z}_n)}{\max|\nabla_z E(\mathbf{z}_n)|}, \quad (21)$$

where \mathbf{z}_n is the vector of airfoil's surface nodal vertical coordinates at iteration n , and γ is a sufficiently small step size. It should be noted that at each iteration, the step that we take in the direction of the gradient is $\frac{\gamma}{\max|\nabla_z E(\mathbf{z}_n)|}$.

This results in an optimal deformation in a local sense, as the gradient shows the direction of maximal increase of E for each iteration; however, as will be shown later, such local optima do not lead to an optimal deformation in a global sense after several iterations. Also care should be taken to choose the value of step size in gradient ascent algorithm. If γ is too small, the convergence will be slow; on the other hand, if it is too large, it is possible that algorithm does not follow the steepest ascent direction. Note that there is no objective function to be minimized in this case as we are solving an unconstrained optimization problem using GA algorithm. At each iteration, as will be explained in the next section, we project the gradient onto a specified waviness profile and take a sufficiently small step in the gradient direction and find the new waviness profile. Then, the algorithm updates the geometry and the grid using the IDWarp package to solve all the direct and adjoint equations for the newly updated airfoil and finds the new gradient. Subsequent iterations are performed until the convergence criteria ΔN is achieved.

4.1.1 Gradient Projection

The wavelengths of potential waviness on airfoils are commonly influenced by factors such as the manufacturing process and their internal structure, particularly for composite panels. Additionally, induced deformations caused by the installation of numerous rivets on the surface panels can also play a role. Consequently, it is more pragmatic to restrict the range of possible wavelengths for the waviness on the airfoil. This can be achieved by projecting the gradient onto a specific basis, thereby narrowing down the feasible options. Considering that, at each iteration, we have projected the gradient onto a basis of k sine Fourier modes as

$$(\nabla_z E)_{pr} = \sum_{n=1}^k \left[b_n \sin\left(\frac{n\pi(\mathbf{x} - x_s)}{x_f - x_s}\right) \right], \quad (22)$$

where the coefficient of each Fourier mode, b_n , is calculated as

$$b_n = \frac{2}{x_f - x_s} \int_{x_s}^{x_f} \nabla_z E(x) \sin\left(\frac{n\pi(\mathbf{x} - x_s)}{x_f - x_s}\right) dx. \quad (23)$$

TOLERANCES FOR NATURAL LAMINAR FLOW DESIGN

Here, \mathbf{x} is the vector of surface nodal coordinates along the chord, and x_s and x_f are the beginning and end of the region that we are modifying the airfoil. We have chosen the Fourier sine basis instead of the complete Fourier series because it enforces that the displacements at the extremes of the function are always zero, i.e., there will be no forward- or backward-facing steps on the airfoil. For the NLF(2)-0415 used in this work, $x_s = 8\%$ and $x_f = 70\%$ of the chord. After projecting the gradient, we use $(\nabla_z E)_{pr}$ in the algorithm.

4.2 SLSQP

As previously mentioned, when employing the gradient ascent method, there is no guarantee that the obtained profile by marching in the gradient direction is the one with the minimum $L2$ -norm that results in the desired ΔN . To address this concern, a constrained optimization problem can be solved. By solving this problem, we can ensure that the profile with the minimum $L2$ -norm, which will increase the maximum value of the N -factor by ΔN units, is attained.

For this, we parameterize the surface using k sine Fourier bases, which also determines the minimum wavelength of waviness on the surface as

$$\mathbf{z} = \mathbf{z}_0 + \sum_{n=1}^k \left[b_n \sin \left(\frac{n\pi(\mathbf{x} - x_s)}{x_f - x_s} \right) \right]. \quad (24)$$

Then, the Fourier coefficients, b_n , are considered as design variables and they are found as the solution to the following optimization problem:

$$\begin{aligned} \min_{\Delta z \in \mathbb{R}} \quad & J = \Delta z_1^2 + \Delta z_2^2 + \dots + \Delta z_{np}^2 \\ \text{w.r.t.} \quad & b_1, b_2, \dots, b_k \\ \text{s.t.} \quad & E = E_{target} = E_R E_0. \end{aligned} \quad (25)$$

Here, J is the objective function that represents the $L2$ -norm of the deformations, $\Delta z_i = z_i - z_{0,i}$ is the vertical surface deviation of the i^{th} node on the surface, np is the number of surface grid nodes to be modified, E is the kinetic energy of disturbances in the boundary layer, E_{target} is the target kinetic energy of disturbance in the boundary layer which corresponds to a specific ΔN , E_0 is the kinetic energy of disturbances in the BL for the clean baseline airfoil, and $E_R = \frac{E_{target}}{E_0}$.

The sequential least squares programming (SLSQP) algorithm from the SciPy²⁵ library is used to solve this constrained optimization problem. To solve equation (25) using SLSQP, the gradients of the objective function and constraint with respect to design variables, i.e., $\frac{dJ}{db_k}$ and $\frac{dE}{db_k}$, are needed. $\frac{dJ}{db_k}$ can be found analytically, using the chain rule, from the definition of the objective function in equation (25) and parameterization of the surface (24) as $\frac{dJ}{db_k} = \frac{dJ}{dz} \frac{dz}{db_k}$. Also, $\frac{dE}{db_k}$ can be calculated, using the chain rule, from gradients of the kinetic energy of perturbation with respect to surface deformation $\frac{dE}{dz}$, which is obtained from the adjoint method, and $\frac{dz}{db_k}$ as $\frac{dE}{db_k} = \frac{dE}{dz} \frac{dz}{db_k}$. Once $\frac{dJ}{db_k}$ and $\frac{dE}{db_k}$ are calculated, they are passed to the optimizer and the optimal values for design variables, b_k , are found and then the waviness profile is reconstructed using equation (24). It is important to highlight a key difference between this approach and gradient ascent. In the gradient ascent method, the algorithm's input and stopping criteria rely on the target ΔN . While the algorithm marches in the direction of the gradient of kinetic energy of perturbations, the value of ΔN is continuously monitored at each iteration until the desired value is reached. On the other hand, in the SLSQP approach, we cannot directly utilize the target ΔN as a constraint. This is because we calculate the gradient of kinetic energy, not the N -factor with respect to surface deformation. Additionally, we need to provide the optimizer with the gradient of the constraint with respect to the design variables. Therefore, we must establish a correlation between the target ΔN and its corresponding kinetic energy of the domain (E_{target}). This correlation can be determined through trial and error by selecting a specific E_{target} and examining the resulting ΔN , or it can be approximated using the results of the gradient ascent method.

4.3 Finding Manufacturing Tolerances

The waviness profiles that are found with gradient ascent and SLSQP algorithms are the largest allowable profiles (and with minimum $L2$ -norm of surface deviations when SLSQP is used) that will increase the maximum growth of convective instabilities by a specific predefined amount, which is defined by ΔN as previously explained. Largest allowable profile with minimum $L2$ -norm of surface deviations implies that any other waviness profile with the same $L2$ -norm is not as worse as that case in terms of amplifying the instabilities inside the boundary layer. Thus, we can

define the tolerance h_{tol} as the $L2$ -norm of surface deviations of the largest allowable deformation profile (for a specific flight condition and k) with respect to the clean airfoil. This can be written as

$$h_{tol} = \sqrt{\frac{1}{(x_f - x_s)} \int_{x_s}^{x_f} (\Delta z_i)^2 dx}, \quad (26)$$

where Δz_i is surface nodal vertical deformation, calculated using SLSQP or GA approaches, for $x \in [x_s, x_f]$.

5. Results

In this part, after introducing the simulation parameters, the effects of Reynolds number, minimum wavelength of waviness, angle of attack (AoA), and selection of the unstable mode on manufacturing tolerances will be investigated. Also, the results obtained with two optimization methods, i.e., gradient ascent (GA) and SLSQP, will be compared.

5.1 Flow Cases and Stability Analysis Parameters

The results were obtained for a Mach number equal to 0.5 for different Reynolds numbers and angles of attack, with thermodynamic properties based on a flight altitude of 9600 meters. For stability analysis of each case, we found the most unstable mode (for baseline airfoil) among a wide range of different feasible modes. Reynolds number (Re), angle of attack (AoA) and the corresponding lift coefficient (C_l) and parameters for stability analysis, including the frequency (f), spanwise wavenumber (β) and the initial value for the complex-valued streamwise wavenumber ($\alpha = \alpha_r + i\alpha_i$) of the most amplified disturbance mode are summarized in table 1.

Table 1: Parameters used for analysis of different cases.

$AoA(^{\circ})$	-0.8240	-0.1340	0.2096	0.550	0.8997	1.25	1.25	1.25
$Re(\times 10^6)$	15	15	15	15	15	15	9	12
C_l	0.50	0.60	0.65	0.70	0.75	0.80	0.80	0.80
$f[Hz]$	9941.81	9822.53	9816.62	9797.17	8382.31	8341.67	7519.06	8172.98
$\beta[m^{-1}]$	247.42	303.53	235.28	230.68	445.99	288.19	223.34	257.40
$\alpha_r[m^{-1}]$	1140.28	1098.20	1083.43	1059.21	894.41	888.20	760.90	847.78
$\alpha_i[m^{-1}]$	2.11	5.44	13.46	7.40	4.97	11.11	-3.75	-6.42

5.2 Effect of Reynolds Number and Wavelength of Waviness

Figure 4 shows the tolerances calculated for $\Delta N \in [0.3, 2]$ with GA and SLSQP approaches. The cases were simulated for $Re \in [9; 12; 15] \times 10^6$, $C_l = 0.8$, and $k \in [10; 16]$. From the two figures, it is clear that increasing the Reynolds number or considering waviness profiles with smaller wavelengths (larger values of k), will decrease the tolerances. The reason behind this is the fact that as Reynolds number increases for the same chord length, the boundary layer gets thinner. As a result, the variations in pressure distribution (C_p) on the airfoil surface due to waviness have a more pronounced effect on the BL characteristics, and instabilities grow faster. In other words, the effect of adverse pressure gradient due to surface waviness which destabilizes the instability waves is more pronounced when the Reynolds number increases. Also, as we decrease the wavelength of waviness on the airfoil, higher levels of adverse-favorable pressure gradient will appear on the surface which decreases the tolerances. The figures also show that, in general, the tolerances which are found using SLSQP are lower than the ones obtained using GA, which is consistent with the properties of the two methods as discussed earlier. The difference between the results obtained with the two methods in most cases is less than 10% and it decreases as we increase the Reynolds number, especially for large wavelengths (lower k).

It should also be mentioned that a convergence study for γ (see equation (21)) was performed to find the acceptable value to be used in GA algorithm. The value of $\gamma = 4 \times 10^{-6}(m)$ turned out to be a good value to guarantee convergence with respect to the step size γ and a reasonable number of iterations. Thus, this value of γ is used for all GA calculations.

TOLERANCES FOR NATURAL LAMINAR FLOW DESIGN

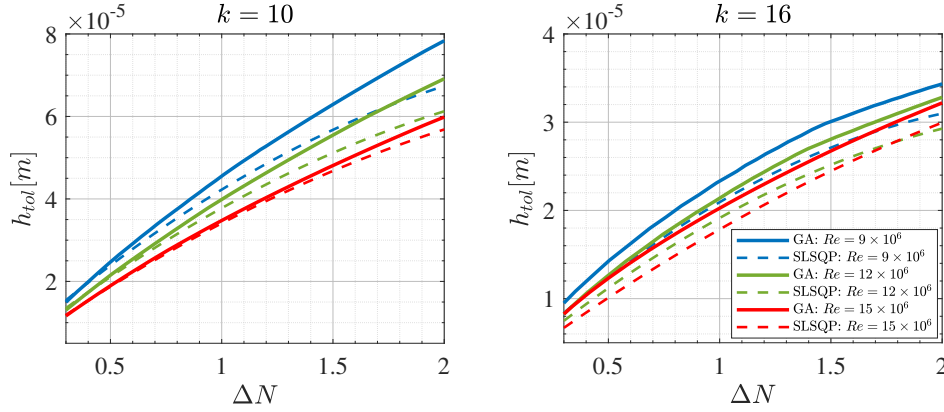


Figure 4: Tolerances computed with GA and SLSQP for $Re \in [9; 12; 15] \times 10^6$, and for $k = 10$ (left panel) and $k = 16$ (right panel) for $C_l = 0.8$ using the corresponding modes in table 1.

5.3 Effect of Angle of Attack

Figure 5 shows the tolerances computed with two methods for $C_l \in [0.5; 0.8]$ at $Re = 15 \times 10^6$ for $k = 10$. From figure 5 it is clear that for the lowest angle of attack, ($AoA = -0.8240^\circ$, $C_l = 0.5$) the results obtained with two methods are almost identical, mainly due to the absence of adverse pressure gradient until $x/c \approx 0.70$ for the upper side of the airfoil, which does not happen for higher lift coefficients. Therefore, for small AoA, i.e., $C_l \leq 0.5$, it is expected to have larger manufacturing tolerances, since the strongly favorable pressure gradient has a stabilizing effect in the boundary layer, requiring larger waviness amplitudes to cause the same variation in the N -factor envelope. The reader should be reminded that the tolerances informed in figure 5 simply imply a maximum $\Delta N = 2$, and do not represent the tolerance for which we have transition associated with the maximum N -factor value. For example, the condition for $C_l = 0.5$ had a maximum N -factor of 4.0 for the clean airfoil, which means the maximum value of h_{tol} in figure 5 corresponds to a N -factor equal to 6.0. In the absence of the experimental or expected N_T associated with the transition, if one chooses the typical value of $N_T = 9$,²⁶ the tolerances would be larger, i.e. $\Delta N = 5$. The condition for $C_l = 0.8$, on the other hand, for the clean airfoil had a maximum N -factor of 14.82, so the maximum tolerance that is informed in figure 5 is associated with $N = 16.82$. Knowing the exact value for N_T is hard, usually requiring wind tunnel experiments or flight tests, once the value of $N_T = 9$ is not universal, depending on the turbulence intensity, and many flight tests have tracked the transition onset for $N_T = 13.5$,²⁷ $N_T = 17.2$,²⁸ and $N_T \approx 20$,²⁹ when the envelope approach is used. Therefore, the present methodology allows the determination of manufacturing tolerances based on acceptable ΔN values to be decided by the aerodynamicist, that will know in advance the maximum expected ΔN that the geometry can produce.

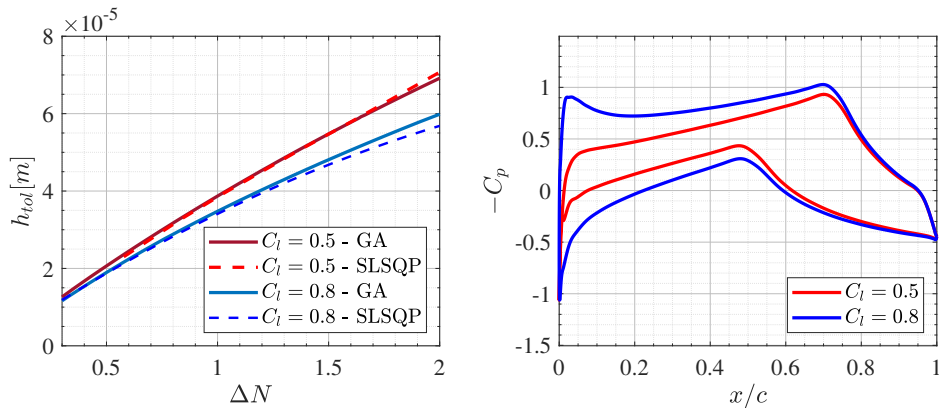


Figure 5: Effect of lift coefficient in the computed tolerances for $Re = 15 \times 10^6$ and $k = 10$.

On what concerns the computational time of both approaches, using the gradient ascent (GA) method, a full curve, like in figure 5, can be generated in less than 5 hours using only four cores, taking 50 to 60 iterations with $\gamma = 4 \times 10^{-6}$ [m] to reach $\Delta N = 2$. Each point of the same curve, i.e., h_{tol} corresponding to each ΔN for a specific

Re and k , using SLSQP can take up to 12 hours (depending on the values of E_R) using the same number of cores. Considering the small difference between the results obtained with the two methods (especially for higher Reynolds number cases), in the next section only the results obtained using the GA algorithm are reported for $Re = 15 \times 10^6$.

5.4 Effect of Mode Selection

As explained in section 2.4, to do the stability analysis we have found the most unstable modes among a wide range of different feasible modes to be used as initial condition in PSE calculations. However, this is not true to claim that the mode which is found is the most amplified mode among all possible modes since we are not able to find an infinity number of instability modes. As was explained in section 2.2.4, in PSE approach, the streamwise wavenumber (unlike in local linear stability analysis) is not constant, and the initial mode serves as the initial condition required to solve PSE with marching algorithm. Moreover, it has been shown that optimizing the measure of kinetic energy based on a single mode, will affect the growth of large number of disturbances³⁰. So if we find the sensitivities based on the most amplified mode that we found, we expect that no other mode will become the most amplified mode during the process. This has been checked during the process and keeping the mode constant turned out to be a good option. However, it might be possible to have several modes with almost the same maximum N -factor but with different frequencies. In that case, a specific mode with slightly lower maximum N -factor might result in lower tolerances due to resulting pressure gradient in the final airfoil shape. Figure 6 shows the maximum N -factor (for clean baseline airfoil) for $Re = 15 \times 10^6$, and for different frequencies in the range of 4000-14000 Hz. For each lift coefficient, the frequency for which the N -factor is maximum is selected as the most amplified mode. From the figure it is clear that for all lift coefficients considered here, there is a highly amplified mode with frequency in range 9699-9822 Hz. However, as the lift coefficient increases (by increasing angle of attack), for $C_l \in [0.75; 0.8]$, another mode which has been used in the results showed earlier in this work and are summarized in table 1, with lower frequency in the range of 8241-8447 Hz becomes more unstable than the previous one. In this case, i.e., when a second mode becomes more unstable, it is important to calculate the tolerances not only based on the most amplified mode, but also with the other less amplified modes that have almost the same maximum N -factor compared to the most amplified one.

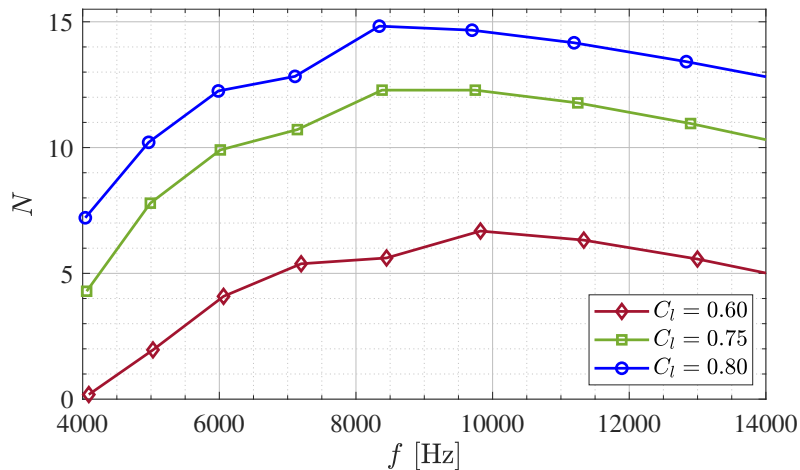


Figure 6: Maximum N -factor (for clean baseline airfoil) for $Re = 15 \times 10^6$, and for different frequencies in the range of 4000-14000 Hz

Figure 7 shows the tolerances (obtained only with gradient ascent as explained in section 5.3), for $\Delta N = 2$, $k = 10$, $Re = 15 \times 10^6$, and $C_l = [0.50; 0.60; 0.65; 0.70; 0.75; 0.80]$. Here, we present two curves for tolerances, one obtained with the most amplified mode found for each case (as reported in table 1), which is shown by the black line in the left panel of the figure, and the other time (shown by dashed red line in the figure), for $C_l = [0.75; 0.80]$, we have found the tolerance based on the second most unstable mode, which has a frequency close to the frequency of most amplified modes for lower lift coefficients as shown in figure 6. The results are shown in the left panel of figure 7. It is clear that if we calculate the tolerances for all lift coefficients based on an initial mode which has a frequency in the range of 8241-8447 Hz, the tolerances decreases by increasing the lift coefficient as expected. However, if for $C_l = [0.75; 0.80]$ we find the tolerances based on the most amplified mode for those cases, the tolerances will be larger than the tolerances for lower lift coefficients. The envelop of N -factor for $C_l = 0.75$, shown in the right panel of

TOLERANCES FOR NATURAL LAMINAR FLOW DESIGN

figure 7, sheds light on the reason behind this. From the envelopes, it is clear that although the maximum N – factor is the same when either of the first or second most amplified mode (which are given in table 2) is used, the variation of N – factor along the chord, which is a direct indication of pressure distribution on the airfoil surface, is different. When the second mode is used, the final optimized shape has a large bump (which means a large adverse pressure gradient) in the upstream position of the chord, where the boundary layer is thinner, and this will result in a lower tolerance compared to the tolerance obtained when the first mode is used.

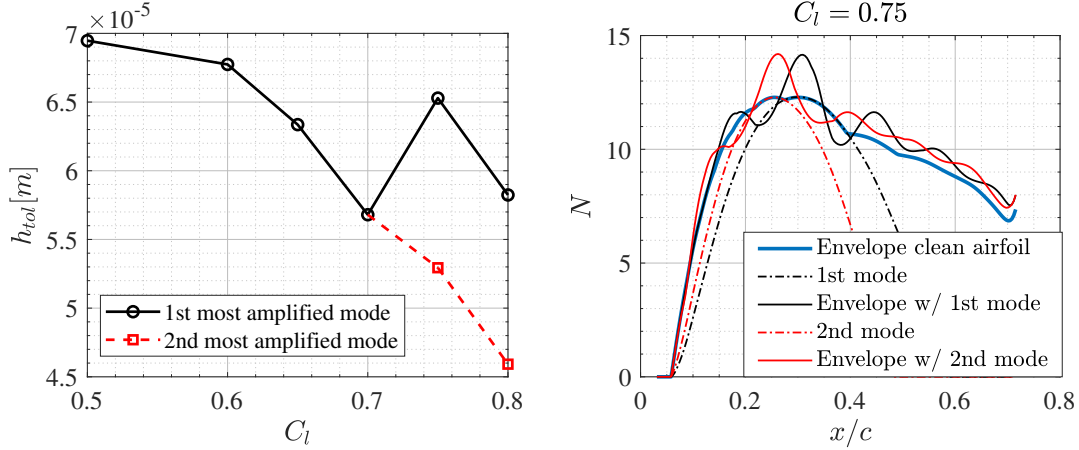


Figure 7: Tolerances using first and second most amplified modes for $k=10$ and corresponding envelopes.

Table 2: First and second most amplified modes for $Re = 15 \times 10^6$.

First most amplified mode					
C_l	$f[s^{-1}]$	β	α_i	α_r	N_{max}
0.75	8382.31	445.99	894.42	4.97	12.298
0.80	8341.67	288.19	888.20	11.11	14.827
Second most amplified mode					
0.75	9746.99	289.79	1028.09	14.66	12.283
0.80	9699.23	288.19	1001.68	1.60	14.666

6. Conclusions

In this work, a methodology to find manufacturing tolerances based on the largest allowable smooth waviness profile on aerodynamic surfaces, which amplifies the convective instabilities in the boundary layer with a prescribed value ΔN , is presented. In order to find the desired waviness profile, two optimization algorithms, i.e., gradient ascent and SLSQP, are used to solve an unconstrained and constrained optimization problem. The method is used to find the manufacturing tolerances for NLF(2)-0415 natural laminar airfoil at Mach number equal to 0.5, and for different Reynolds numbers and wavelengths of waviness on airfoil, and at different angles of attack. The results indicate that increasing the Reynolds number and using waviness profiles with smaller wavelengths lead to a decrease in the tolerances needed to maintain laminar flow. However, as the angle of attack decreases, the tolerance increases due to a larger extent of favorable pressure gradient region on the airfoil. It also has been shown that the SLSQP is the method capable of finding the largest allowable deformation profile with a minimum $L2$ -norm of surface deformation, at the cost of additional computational time compared to the GA approach, which informs tolerances within an error of less than 15% but in a shorter time frame. It should be noted that the tolerances are dependent on the perturbation mode which is used for the stability calculations. Although using the most amplified mode for the baseline airfoil in the whole

optimization process is a good choice, it is recommended to find the tolerances based on other perturbation modes as well.

The methodology proposed here expresses the efforts made to obtain manufacturing tolerances for NLF surfaces for aerodynamic applications, where the advantage of the proposed methodology is the extra information that is given at the beginning of the process, i.e., the final ΔN that the manufactured geometry will result. This helps engineers dictate manufacturing tolerances with more confidence about their effects.

7. Acknowledgments

This project received funding from the European Union's Horizon 2020 research and innovation programme under the Marie Skłodowska-Curie grant agreement No 955923. The authors also would like to thank CNPq, Embraer, and CISB for funding and supporting the work on the Brazilian side.

References

- [1] European Commission, *Flightpath 2050 - Europe's vision for aviation*, Office of the European Union, 2011.
- [2] A. H. Epstein, "Aeropropulsion for commercial aviation in the twenty-first century and research directions needed," *AIAA Journal*, vol. 52, no. 5, pp. 901–911, 2014.
- [3] D. King, O. Inderwildi, and C. Carey, "Advanced aerospace materials: past, present and future," *Aviat Environ (Paris Airshow Spec Ed)*, vol. 3, pp. 22–27, 01 2009.
- [4] R. Peoples and K. Willcox, "Value-based multidisciplinary optimization for commercial aircraft design and business risk assessment," *Journal of Aircraft*, vol. 43, no. 4, pp. 913–921, 2006.
- [5] F. Collier, "Concepts and technologies for green aviation," Sep. 2009.
- [6] G. Schrauf, "Status and perspectives of laminar flow," *The Aerospace Journal*, vol. 109, pp. 639–644, Dec. 2005.
- [7] W. S. Saric, H. L. Reed, and E. B. White, "Stability and transition of three-dimensional boundary layers," *Annual review of fluid mechanics*, vol. 35, no. 1, pp. 413–440, 2003.
- [8] A. Fage, "The smallest size of a spanwise surface corrugation which affects boundary-layer transition on an aerofoil," 1943.
- [9] B. H. Carmichael, "'surface waviness criteria for swept and unswept laminar suction wings.," Tech. Rep. NOR 59-438, Norair, 1959.
- [10] J. Crouch, "Modeling transition physics for laminar flow control," in *38th Fluid Dynamics Conference and Exhibit*, p. 3832, 2008.
- [11] J. Perraud, H. Deniau, and G. Casalis, "Overview of transition prediction tools in the elsa software," in *ECCOMAS 2014*, 2014.
- [12] Y.-S. Wie and M. R. Malik, "Effect of surface waviness on boundary-layer transition in two-dimensional flow," *Computers & fluids*, vol. 27, no. 2, pp. 157–181, 1998.
- [13] O. Amoignon, J. Pralits, A. Hanifi, M. Berggren, and D. Henningson, "Shape optimization for delay of laminar-turbulent transition," *AIAA journal*, vol. 44, no. 5, pp. 1009–1024, 2006.
- [14] C. A. Mader, G. K. Kenway, A. Yildirim, and J. R. Martins, "Adflow: An open-source computational fluid dynamics solver for aerodynamic and multidisciplinary optimization," *Journal of Aerospace Information Systems*, vol. 17, no. 9, pp. 508–527, 2020.
- [15] A. Yildirim, G. K. Kenway, C. A. Mader, and J. R. Martins, "A jacobian-free approximate newton–krylov startup strategy for rans simulations," *Journal of Computational Physics*, vol. 397, p. 108741, 2019.
- [16] S. Hein, F. Bertolotti, M. Simen, A. Hanifi, and D. Henningson, "Linear nonlocal instability analysis-the linear nolot code," 1995.
- [17] J. O. Pralits, C. Airiau, A. Hanifi, and D. S. Henningson, "Sensitivity analysis using adjoint parabolized stability equations for compressible flows," *Flow, turbulence and combustion*, vol. 65, pp. 321–346, 2000.

TOLERANCES FOR NATURAL LAMINAR FLOW DESIGN

- [18] F. Bertolotti and T. Herbert, “Analysis of the linear stability of compressible boundary layers using the pse,” *Theoretical and Computational Fluid Dynamics*, vol. 3, no. 2, pp. 117–124, 1991.
- [19] J. Van Ingen, “The en method for transition prediction. historical review of work at tu delft,” in *38th Fluid Dynamics Conference and Exhibit*, p. 3830, 2008.
- [20] D. M. Somers and K.-H. Horstmann, “Design of a medium-speed natural-laminar-flow airfoil for commuter aircraft applications,” *DFVLR IB*, pp. 129–85, 1985.
- [21] D. Prosser, “Construct2d, <https://sourceforge.net/projects/construct2d/>.”
- [22] G. K. Kenway, C. A. Mader, P. He, and J. R. Martins, “Effective adjoint approaches for computational fluid dynamics,” *Progress in Aerospace Sciences*, vol. 110, p. 100542, 2019.
- [23] R. M. Hicks and P. A. Henne, “Wing design by numerical optimization,” *Journal of Aircraft*, vol. 15, no. 7, pp. 407–412, 1978.
- [24] N. R. Secco, G. K. Kenway, P. He, C. Mader, and J. R. Martins, “Efficient mesh generation and deformation for aerodynamic shape optimization,” *AIAA Journal*, vol. 59, no. 4, pp. 1151–1168, 2021.
- [25] P. Virtanen, R. Gommers, T. E. Oliphant, M. Haberland, T. Reddy, D. Cournapeau, E. Burovski, P. Peterson, W. Weckesser, J. Bright, *et al.*, “Scipy 1.0: fundamental algorithms for scientific computing in python,” *Nature methods*, vol. 17, no. 3, pp. 261–272, 2020.
- [26] A. M. O. Smith and N. Gamberoni, “Transition, pressure gradient and stability theory,” Tech. Rep. Rep. ES 26388, Douglas Aircraft Company, Long Beach, Calif., 1956.
- [27] A. Q. K. H. Horstmann and G. Redeker, “Flight and wind-tunnel investigations on boundary-layer transition,” *J. Aircraft*, vol. 27, no. 2, pp. 146–150, 1990.
- [28] C. Obara and B. Holmes, “Flight-measured laminar boundary-layer transition phenomena including stability theory analysis,” *NASA technical paper ; 2417.*, 05 1985.
- [29] R. A. Rozendaal, “Variable sweep transition flight experiment (vstfe)-stability code development and clean-up glove analysis,” Tech. Rep. CP 2487, Part 3, NASA, Hampton, 1987.
- [30] J. O. Pralits and A. Hanifi, “Optimization of steady suction for disturbance control on infinite swept wings,” *Physics of fluids*, vol. 15, no. 9, pp. 2756–2772, 2003.